Influences of Loading Rate and Preloading on the Mechanical Properties of Dry Elasto-Plastic Granules Under Compression

Alexander Russell, Peter Müller, Hao Shi, and Jürgen Tomas
Mechanical Process Engineering, Institute of Process Engineering, Otto von Guericke University of Magdeburg, Universitätsplatz 2, 39106 Magdeburg, Germany

DOI 10.1002/aic.14572
Published online August 14, 2014 in Wiley Online Library (wileyonlinelibrary.com)

To ensure high quality of granular products post-industrial operations, it is necessary to precisely define their micro–macro mechanical properties. However, such an endeavor is arduous, owing to their highly inhomogeneous, anisotropic and history-dependent nature. In this article, we present the distributed granular micromechanical and macromechanical, energetic and breakage characteristics using statistical distributions. We describe the material behavior of elasto-plastic zeolite 4AK granules under uniaxial compressive loading until primary breakage, and localized cyclic loading up to different maximum force levels, at different displacement-controlled loading rates. The observed force-displacement behavior had been approximated and further evaluated using well-known contact models. The results provide the basis for a detailed analysis of the viscous behavior of zeolite 4AK granules in the moist and wet states, indicating that higher compressive loads are required at higher displacement-controlled loading rates to realize equivalent deformation and breakage probability achieved by loads at lower displacement-controlled loading rates. © 2014 American Institute of Chemical Engineers *AIChE J*, 60: 4037–4050, 2014
Keywords: breakage, compression, deformation, granules, mechanical properties

Introduction

According to a survey reported almost a couple of decades ago, granular products account to 60% of final products in the chemical industry alone, with an annual economic value of almost US$ 1 trillion in the US alone.[1] With the diversified and increasing requirements of today's global market, one can only predict that the economic value may have drastically increased. Granulated products, that is, granules are inhomogeneous complex particle–particle compounds (semi-permanent aggregates of size 100 μm or larger), composed of individually identifiable solid primary particles (fine to ultrafine powders of size ranging from 1 to 100 μm) and processing additives such as binders, bonded together by adhesive forces, liquid or solid bridges. They are traditionally preferred ahead of their constituents, that is, powders, due to their better flowability mixability, permeability, dispersion and dissolution, easier handling and classification, lesser segregation, reduced dust formation and material losses, as well as flow resistance and sintering temperature, and well-defined physical properties such as size, shape, density, porosity, composition, and stability.[2,3] Nevertheless, they also possess disadvantages such as non-uniform, anisotropic, and history-dependent mechanical behavior which often results in undesired breakage leading to fragmentation producing fines and dust.

Corresponding concerning this article should be addressed to A. Russell at alexander.russell@ovgu.de.

In general, granules are processed in continuous modes, handled, transported, and stored as bulk solids, during which the granule bed may be subjected to quasi-static stressing (see Figure 1), for example, in storage silos, catalyst reactors, adsorption column packings, and so forth, and dynamic stressing, for example, in centrifuges, discharge hoppers, pneumatic conveying, and so forth. However, in every industrial practice, processes often advance at low granule concentrations, for example, dilute-phase pneumatic conveying, apparatus filling, and so forth. At such conditions, individual granules are stressed (see Figure 1) under varying strain rates. Due to such stressing events, granules may deform and undergo attrition and/or breakage.

In comminution processes, breakage of total granule population with a minimal stressing energy input is desired, whereas to avoid undesired product failure by breakage, handling processes are required to advance such that the stressing energy input falls below the minimum energy required to initiate breakage (see Figure 2). Nevertheless, during comminution processes, there is limited control over breakage of individual granules, thus, the stressing energy input may be substantially higher than the minimum required to initiate desired breakage. Similarly, during handling processes, the stressing energy input may be substantially sufficient to initiate undesired breakage of individual granules. To design industrial equipment and corresponding operations with granules (be it for comminution or handling purposes), it is necessary to precisely evaluate their micro-yield and macro-breakage probability, for example, eventually, defining clear cut-off energy requirements to initiate micro-yield and macro-breakage. As, such precise definitions of the energy requirements are arduous to represent,

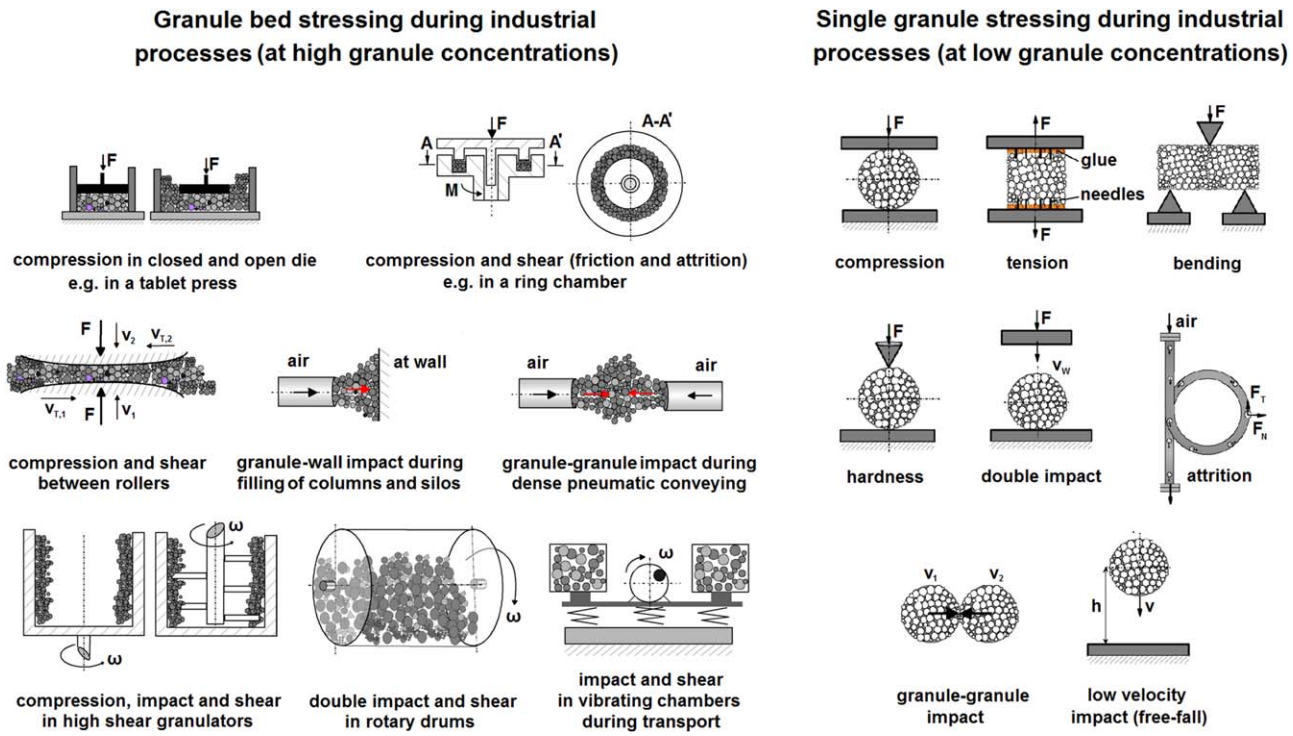

Figure 1. Stressing of granule beds and single granules during industrial processes.[4,5]

[Color figure can be viewed in the online issue, which is available at wileyonlinelibrary.com.]

mostly a "trial-and-error" approach is followed in industrial operations with granules.

To progress toward solving this industrial problem, the distributed mechanical properties and predictable limits of the micro–macro constitutive relationship with respect to material properties (microscopic: primary particulate content, interparticulate interactions, binder material content, and solid bridge strength; and macroscopic: size, shape, and density), and process conditions (humidity, time of contact, point of contact, intensity and frequency of stressing events) are necessary. In previous communications,[6–10] we have extensively described the influences of granule size, humidity (represented by moisture content), stressing intensity (represented by loading force), and frequency (represented by number of loadings) on the material behavior of model elasto-plastic granules under uniaxial compression. In this article, we present the effects of displacement-controlled loading rates on the material behavior under uniaxial compression.

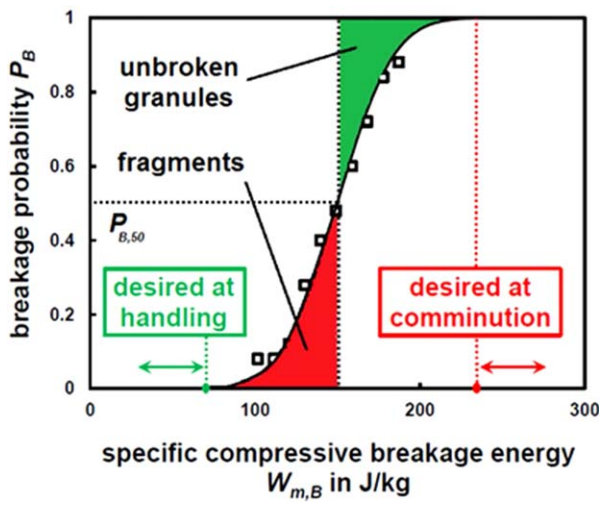

Figure 2. The statistically distributed breakage probability of a certain granule population.

[Color figure can be viewed in the online issue, which is available at wileyonlinelibrary.com.]

In principle, the effect of loading rate arises from the difference in the velocity of stress wave propagation throughout the entire volume of the granule during loading and unloading. Thus, at different loading rates, a clear difference may be observed in the realized deformation and/or breakage of the granule. Furthermore, according to Gorham,[11] Vogel and Peukert,[12] and Zhang and Wong,[13] as larger granules have to be compressed at proportionately higher displacement-controlled loading rates to achieve equivalent strain rates as for smaller granules, it is thus expected that a higher stressing energy input is required to achieve an equivalent deformation or breakage probability of a large granule in comparison to a smaller one. Nevertheless, this difference is significant only in case of dominantly viscous granules.

Similarly, the nucleation and propagation of initial (ring and radial) cracks in the elastically and the plastically deformed annular and central zones, respectively (see Schönert[14] and Tomas et al.[15]), may occur at different rates directly correlating with the corresponding loading rate. According to Rumpf,[16] Tavares and King,[17] Tavares,[18] and Qi et al.,[19] different rates of crack propagation primarily correlate with different rates of deformation, and eventually affects the breakage probability. Moreover, as shown by Salman and Gorham[20] and Tang et al.,[21] each stress wave in itself does not propagate with a uniform velocity, due to the presence of structural inhomogeneous locations such as pores, solid bridge bonds, micro-cracks, and defects within

Table 1. Historical Survey of Investigations Reported on the Compression Behavior of Granules

Authors	Material	Size Fraction in mm	Loading Rate in mm/s
Iveson[23]	Soda-lime glass spheres	0.01–0.09	0.01, 1, 10, 30, 100, and 150
Salman and Gorham[20]	Soda-lime glass spheres	0.40–12.70	0.0008
Couroyer et al.[24]	Catalyst alumina beads	1.70–2.00	1, 10, and 100
Franks and Lange[25]	Saturated alumina compacts	1.80–2.00	0.008, 0.01, 0.08, and 0.3
Khanal[26]	Concrete agglomerates	150.00	1000
Cheong et al.[27]	Binderless polystyrene particles	3.35–4.00	0.0001, 0.001, 0.01, and 0.1
Samimi et al.[28]	Detergent granules	1.00–2.00	0.001–0.008
Al Mahdi et al.[29]	Dried milk and wheat flour capsules	30.00	0.1
Antonyuk[5]	Zeolite 13X granules	0.90–1.70	0.02, 0.08, and 0.15
Smith[30]	Soda-lime glass spheres	0.02–0.09	0.1, 1, 10, 100, and 180
	Lactose granules	0.04–0.15	
Nguyen et al.[31]	Calcium alginate microspheres	0.08–0.13	0.01–1
Aman et al.[32]	Soda-lime glass spheres	0.60–3.50	4.5 and 9
	Salt, basalt, sugar, and marble particles	1.25–5.00	
Müller[33]	Zeolite 4AK granules	1.00–3.00	0.02
Wiącek et al.[34]	Piast chicken pea particles	6.90–8.00	0.005
	Komosa bean particles	5.40–12.20	
Hanley et al.[35]	Infant formula food agglomerates	0.71–0.85	0.01
Portnikov et al.[36]	Salt particles	2.00–4.00	0.005
	Soda-lime glass spheres	0.71–3.35	

the granular volume. In addition to such volumetric inhomogeneity, granules also exhibit superficial inhomogeneity with varying roughness and curvature, thereby making the determination of the micromechanical properties, the energetic quantities, and the breakage probability highly unpredictable with a large scatter.

Khandelwal and Ranjith[22] suggested that the deformation and breakage realized in coarse agglomerates (such as rock, concrete, etc.) are due to unstable crack propagation following stable crack growth. The authors showed that at higher displacement-controlled loading rates, agglomerates exhibit a higher modulus of elasticity, and higher loads are required to achieve breakage in comparison to the same at lower displacement-controlled loading rates. Comprehensive reviews on the investigations done, to understand the compression behavior of coarse agglomerates, at different loading rates, have been given by Zhang and Wong[13] and Khandelwal and Ranjith.[22] However, such results have not yet been evaluated for granules, that is, millimeter-sized agglomerates.

Although, several works (see Table 1) have been reported on the material behavior of individual granules compressed under different displacement-controlled loading rates, a comparative analysis pointing out the influences of the loading rate has not yet been furnished. This article presents evaluations which point out the influences of the displacement-controlled loading rate on the micromechanical and macromechanical properties. Further novel aspects such as, determination of an energetic coefficient of restitution for simulating mechanical processes where compressive stresses dominate, influences of strain hardening during reloading of a preloaded granule, and identification of the so-called "Bauschinger effect" during unloading of a loaded granule are also described in this article.

Experimental

Materials and methods

As experimental material, zeolite (alumina silicate crystals containing a sodium ion) granules of the type 4AK produced by Chemiewerk Bad Köstritz had been selected. They are characteristically elasto-plastic, almost spherical, highly hygroscopic, water insoluble granules. They are produced by pelletizing, that is, by wet granulation of fine zeolite powder with solid mineral binder attapulgite and other potentially important additives (see Schumann et al.[37]). Following granulation, the produced granules are thermally dried and activated at a temperature of 550°C, during which the binder consolidates and forms a matrix in which the primary particles are embedded in. The granules are widely known as molecular sieves (due to their well-defined pore network) and are used for the desiccation of air-conditioners in automobiles, hydrogen, oxygen, air, organic solvents, hydrogen purification, insulating glass, control of moisture in packages, and conservative bags. Furthermore, they are used as additives in the manufacture of detergents, cosmetic masks, creams, and as adsorbents for the removal of hydrocarbons, ammonia, and methanol from gas streams. Due to such extensively wide applications, zeolite 4AK granules are widely used in industrial sectors, such as in gas processing, package production, automotive, cosmetic, chemical, petrochemical, glass and white good industries.

The structural inhomogeneity of zeolite 4AK granules have been reported using scanning electron microscopy and micro-computed tomography by Müller et al.[9] and Russell et al.,[10] respectively. For the study described herein, two granule size fractions of 1.25–2.24 mm and 2.50–4.00 mm had been selected. The granule-size distribution on the mass basis is presented in Figure 3 while their granulometric and physical properties are presented in Table 2.

Individual granules had been tested by uniaxial compressive monotonic loading until primary breakage and cyclic loading (at a unique contact) up to different defined maximum force levels F_m in measures of the yield force F_y (which is approximately equal to 8 N and 10 N for 1.75 and 3.01 mm sized ranged granules respectively). The 1.75 mm size ranged granules were tested by maximum compressive force levels of 0.5 F_y, 1 F_y, and 1.5 F_y, while the 3.01 mm size ranged granules were tested with 0.4 F_y, 0.8 F_y, 1.2 F_y,

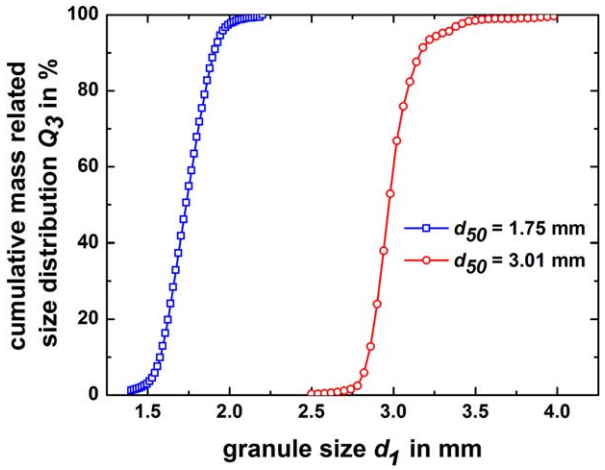

Figure 3. Granule size distribution on the mass basis.

[Color figure can be viewed in the online issue, which is available at wileyonlinelibrary.com.]

and 1.6 F_y. All tests were performed at different constant displacement-controlled loading rates of $v_L = 0.01$, 0.02, 0.08, and 0.15 mm/s. A schematic representation of the performed single granule uniaxial compression tests between two flat and stiff contacts (walls) is shown in Figure 4. To achieve statistically representative results, measurements of at least 25 individual granules (per series) under cyclic loading and at least 100 individual granules (per series) under monotonic loading, had been evaluated. The selected number of individual granules are sufficient to achieve representative results for the described tests due to their narrow-size distributions (see Figure 3), their sphericity (see Table 2) and previous communications[6–10] which describe their mechanical properties with a standard deviation lesser than 15%.

Results and Discussion

Micromechanical properties

The observed experimental force-displacement behavior had been approximated and further evaluated to determine the micromechanical properties. A simple linear approximation of elasto-plasticity had been applied in analogy with the linear Walton–Braun model[38] according to

$$F_L = k_L s \tag{1}$$

Table 2. Granulometric and Physical Properties of Model Zeolite Granules

Content	Primary Particles: Zeolite 83%	Binder: Attapulgite 17%
Chemical composition	$Na_2O{\cdot}Al_2O_3{\cdot}2SiO_2{\cdot}nH_2O$	$(Mg,Al)_2{\cdot}Si_4O_{10}{\cdot}OH{\cdot}4H_20$
Granule size (mean diameter) d_{50} in mm	1.75	3.01
Sphericity ψ	0.98	0.98
Solid (true) density ρ_s in kg/m^3	2,290.7	2,374.7
Granule density ρ_g in kg/m^3	1,127.9	1,102.0
Porosity ε in %	50.76	53.59
Specific surface area S_m in m^2/kg	38.13	44.25

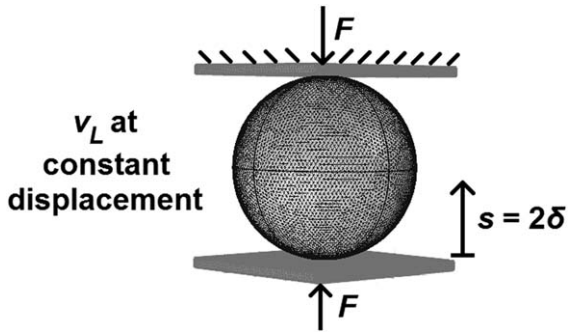

Figure 4. Schematic representation of single granule uniaxial compression tests.

$$F_U = k_U(s - s_m) \tag{2}$$

with F_L and F_U the contact forces at loading and unloading, k_L and k_U the contact stiffnesses at loading and unloading, s the displacement, and s_m the displacement corresponding to maximum applied force.

Similarly, a non-linear approximation of the force-displacement curve had also been applied. The elastic loading regime had been approximated using the non-linear Hertz model,[39] which assumes the contact pressure to be elliptically distributed within the circular contact zone. With the subscripts 1 and 2, respectively, representing the two contact partners, that is, the granule and the wall, the force-displacement relationship during elastic loading of a spherical granule between two flat and stiff walls can be expressed as

$$F_{el} = \frac{2}{3}E^*\sqrt{R^*\left(\frac{s}{2}\right)^3} \approx \frac{4}{3}\frac{E_1}{\left(1-\nu_1^2\right)}\sqrt{R_1\left(\frac{s}{2}\right)^3} = \frac{1}{3}\frac{E_1}{\left(1-\nu_1^2\right)}\sqrt{d_1 s^3} \tag{3}$$

with F_{el} the elastic contact force, s the total deformation of the granule between the two contacts (walls) which is assumed as twice the deformation at one contact δ, and ν the Poisson's ratio which is assumed to be equal to 0.3 (see Antonyuk[5]).

E^* the effective modulus of elasticity of both contact partners within the self-equilibrating elastic contact is given by[40,41]

$$E^* = 2\left[\frac{\left(1-\nu_1^2\right)}{E_1} + \frac{\left(1-\nu_2^2\right)}{E_2}\right]^{-1} \approx \frac{2}{\left(1-\nu_1^2\right)}E_1 \text{ when } E_2 \rangle\rangle E_1 \tag{4}$$

and R^* the effective radius of curvature of both contact partners (characterizing the mean surface curvature of both contact partners prior contact flattening) is given by

$$R^* = \left(\frac{1}{R_1} + \frac{1}{R_2}\right)^{-1} \approx R_1 \text{ when } R_2 \to \infty. \tag{5}$$

The elastic contact stiffness k_{el} follows from the first spatial derivative of the elastic contact force (gradient of the force-displacement curve until maximum elastic load) according to

$$k_{el} = \frac{dF_{el}}{ds} \approx E^*\sqrt{\frac{1}{8}R^* s} = \frac{1}{2}\frac{E_1}{\left(1-\nu_1^2\right)}\sqrt{d_1 s} \tag{6}$$

with E_1 the modulus of elasticity of the granule, equal to the gradient of the linear regime in the so-called linearized Hertzian plot (see Figure 5b), obtained by plotting the quantity $3F(1-\nu_1^2)/d_1^{1/2}$ as a function of $s^{3/2}$.

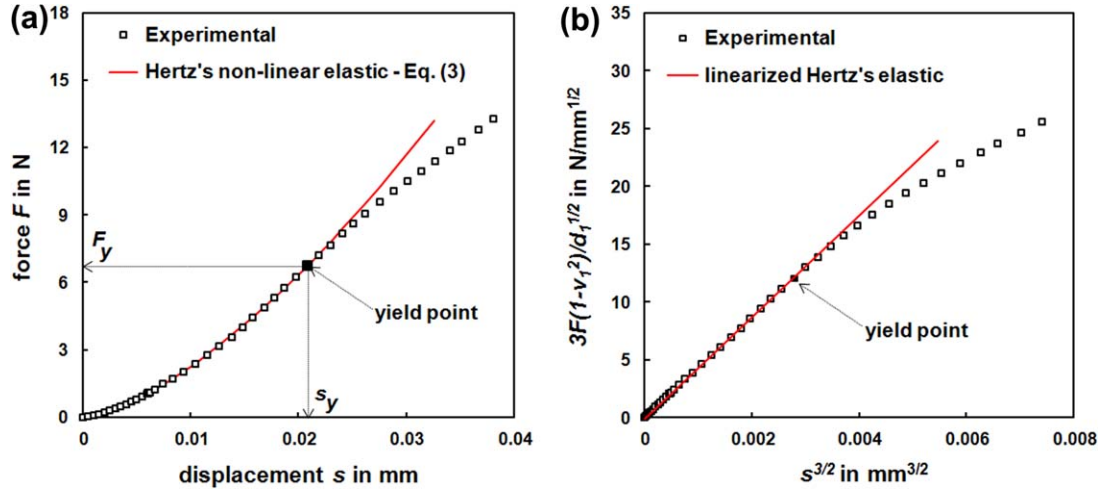

Figure 5. Characteristic (a) loading curve and (b) its corresponding linearized Hertzian plot.

[Color figure can be viewed in the online issue, which is available at wileyonlinelibrary.com.]

From the deviation of the experimental values away from the linearized Hertzian elastic region, the yield point, that is, onset of incipient plastic yielding at the central contact zone can be identified and the characteristic elastic limits, yield force F_y and yield displacement s_y can be noted by correlating with the corresponding force-displacement curve. As the curve resembles a straight line from the origin until the elastic limit, that is, yield point, its gradient is thus constant within this regime. Therefore, the modulus of elasticity at applied maximum compressive loads below the elastic limit (such as 0.5 F_y in case of 1.75 mm; 0.4 F_y and 0.8 F_y in case of 3.01 mm size ranged granules) had been determined from the gradient of the linearized curve until maximum load.

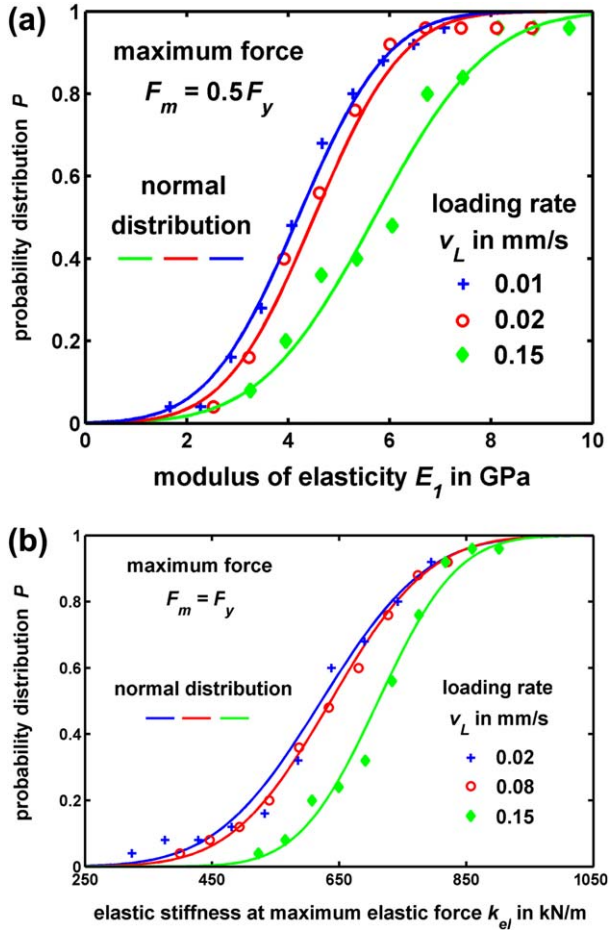

Figure 6. Observed trends of (a) the modulus of elasticity and (b) the elastic stiffness at maximum elastic forces determined under cyclic loading at different loading rates in a granule of size d_{50} = 1.75 mm.

[Color figure can be viewed in the online issue, which is available at wileyonlinelibrary.com.]

Figure 6 presents distributions of the fundamental micromechanical properties within the elastic range, that is, modulus of elasticity and the elastic stiffness at maximum elastic loads, determined under cyclic loading at different loading rates.

Subsequently, the elasto-plastic loading regime (where irreversible plastic yielding initiates at the central contact zone and expands to the annular periphery which continues to deform elastically at substantially lower stresses) had been approximated using the non-linear model of Tomas[42] according to

$$F_{\mathrm{el-pl}} = \frac{3}{2}\lambda_{\mathrm{el-pl}}\kappa_{\mathrm{A}}F_{\mathrm{y}}\left(\frac{s}{s_{\mathrm{y}}}\right) = \frac{1}{4}\pi\lambda_{\mathrm{el-pl}}p_{\mathrm{y}}d_1\left(1-\frac{1}{3}\sqrt[3]{\frac{s_{\mathrm{y}}}{s}}\right)\mathrm{s} \quad (7)$$

with $\lambda_{\mathrm{el\text{-}pl}}$ as a fitting parameter of the model (see Müller[33]).

The displacement-dependent dimensionless contact area ratio κ_{A}, represents the contribution of the inner circular plastically yielding contact area A_{pl} to the total deformation area A_{tot} including an annular elastic deformation according to[43,44]

$$\kappa_{\mathrm{A}} = \frac{2}{3} + \frac{1}{3}\frac{A_{\mathrm{pl}}}{A_{\mathrm{tot}}} = 1 - \frac{1}{3}\sqrt[3]{\frac{s_{\mathrm{y}}}{s}} \quad (8)$$

and the compressive micro-yield strength p_{y} (boundary of compressive strength, at which irreversible plastic yielding initiates) is given by

$$p_{\mathrm{y}} = \frac{6}{\pi}\frac{F_{\mathrm{y}}}{s_{\mathrm{y}}d_1}. \quad (9)$$

The elasto-plastic contact stiffness $k_{\mathrm{el\text{-}pl}}$ follows from the first spatial derivative of the elasto-plastic contact force according to

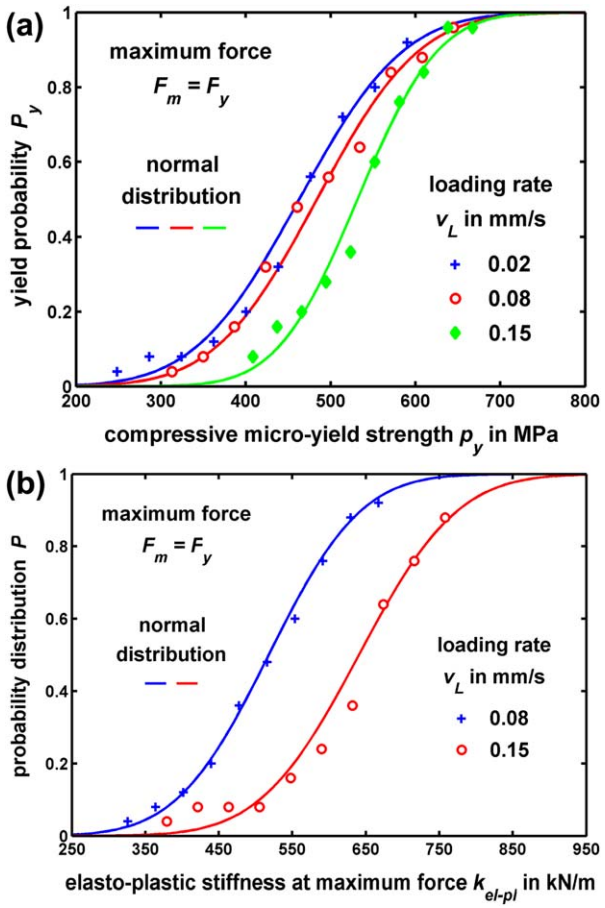

Figure 7. Observed trends in (a) the compressive micro-yield strength and (b) the elasto-plastic stiffness during cyclic loading at different loading rates in a granule of size $d_{50} = 1.75$ mm.

[Color figure can be viewed in the online issue, which is available at wileyonlinelibrary.com.]

$$k_{\mathrm{el-pl}} = \frac{dF_{\mathrm{el-pl}}}{ds} = \frac{1}{4}\pi p_{\mathrm{y}} d_1 \left(1 - \frac{2}{9}\sqrt[3]{\frac{s_{\mathrm{y}}}{s}}\right) \tag{10}$$

Figure 7 presents distributions of the fundamental mechanical properties in the elasto-plastic regime, that is, the micro-yield strength and the elasto-plastic contact stiffness at maximum load determined at different loading rates.

Considering significant elasto-plastic deformation during loading, the elastic limits of the granule may be altered, due to rearrangement of structural inhomogeneities within the central plastically yielding contact zone (independent of the change in curvature). Eventually, facilitating a local hardening, in the direction of the maximum principal strain, thereby causing an increase in the modulus of elasticity. Figure 8a represents a comparison of the moduli of elasticity of granules during loading and unloading determined using the so-called linearized Hertzian plot. Interestingly, the observed modulus of elasticity during unloading is significantly lower than the same which had been observed during loading. The reason being, that the stress state differs significantly, considering the granule relaxing in the normal direction, opposing the transverse strain resulting due to the confined contact force. This phenomenon is best explained by the well-known Bauschinger effect, where the micro-yield strength that withstands compressive and tensile stresses vary inversely, at the expense of each other. However, on reloading, a higher modulus of elasticity than the previous loading cycle can be observed (see Figure 8a), due to strain hardening, as predicted in previous communications.[7,10] Figure 8b presents the modulus of elasticity observed during unloading at different loading rates.

Moreover, apart from the yielding of surface asperities, no significant influence on the granule shape (curvature) occurs (see Figure 9). Therefore, the unloading regime was approximated using a non-linear model in analogy with the Hertzian approach,[39] considering so-called healing contacts, that is, an unchanged curvature of the stressed contacts, according to

$$F_{\mathrm{el,U}} = \frac{1}{3}\vartheta_{\mathrm{el,U}} \frac{E_{1,\mathrm{U}}}{\left(1-\nu_1^2\right)} \sqrt{d_1 (s - s_{\mathrm{U}})^3} \tag{11}$$

with $F_{\mathrm{el,U}}$ the elastic unloading force at contact, s_{U} the residual displacement after complete unloading corresponding to

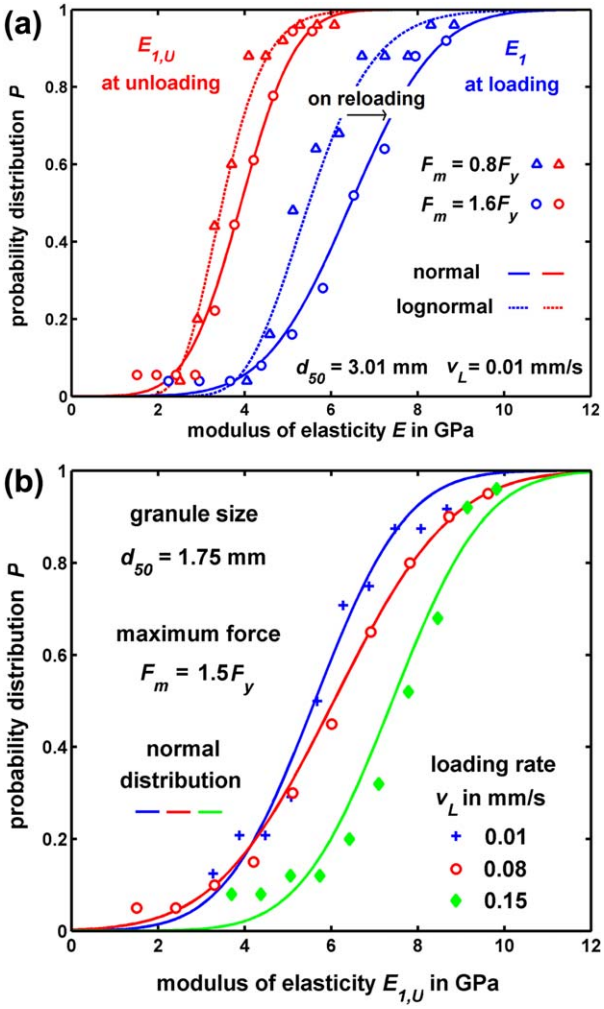

Figure 8. (a) Comparison of the moduli of elasticity during loading and unloading, and (b) the observed trend in the modulus of elasticity during unloading of loaded granules at different loading rates.

[Color figure can be viewed in the online issue, which is available at wileyonlinelibrary.com.]

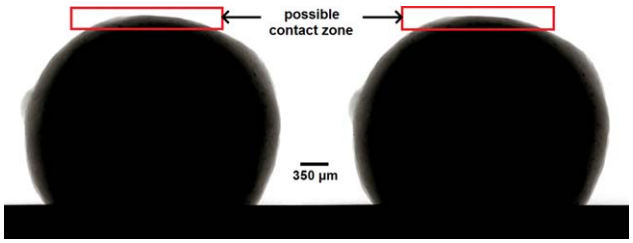

Figure 9. µ-CT images of a granule of size $d_{50} = 3.01$ mm (a) prior loading and (b) after localized cyclic loading with $F_m = 0.4$, 0.8, 1.2, and 1.6 F_y.

[Color figure can be viewed in the online issue, which is available at wileyonlinelibrary.com.]

zero normal force and $\vartheta_{el,U}$ as the fitting parameter of the model that considers additional displacements due to apparent viscoelastic effects and adhesive contacts during pull-off of the stressing walls after complete unloading.

Figures 6–8 clearly show the distributed mechanical properties of the tested zeolite 4AK granules and also present a basis to understand the effects of loading rate on them. Furthermore, Figure 10 shows a characteristic force-displacement curve observed during a complete cycle of loading–unloading approximated with the described linear and non-linear contact models. Table 3 summarizes the parameters used for curve fitting.

Energetic coefficient of restitution

A qualitative parameter to describe the deformation realized in a granule during any dynamic stressing event is the coefficient of restitution e. It is a dimensionless ratio of the final impulse of the granule in the decompression, that is, restitution phase after impact and the first impulse of the granule in the compressive phase during impact. However, an energetic coefficient of restitution e_E may be determined for quasi-static stressing events, by directly correlating the ratio of impulses to a ratio of strain energies (as the mass remains constant before and after the event), and in turn to a ratio of the contact stiffnesses (following the Walton–Braun[38] approach) according to

$$e = \frac{|v_r|}{|v_i|} = \sqrt{\frac{W_{kin,r}}{W_{kin,i}}} \approx e_E = \sqrt{\frac{W_{el,U}}{W_{tot}}} = \sqrt{\frac{\int_{s_m}^{s_U} k_U (s - s_U) ds}{\int_{s_U}^{s_m} k_L s ds}} \approx \sqrt{\frac{k_U}{k_L}} \tag{12}$$

with v the velocity, W_{kin} the kinetic energy, $W_{el,U}$ the elastic strain energy restored during unloading, W_{tot} the total strain energy absorbed during loading, and the subscripts i and r representing the impact and restitution phases of the dynamic stressing event. The strain energies had been determined by spatially integrating the corresponding force-displacement functions.

In previous communications,[7,10] we have furnished that the energetic coefficient of restitution within the elastic and elasto-plastic ranges is independent of the granule size; but dominantly dependent on its pre-stressing history. Similarly, it has also been experimentally observed in this study, that the energetic coefficient of restitution is independent of the constant stressing (loading and subsequent unloading) rate, eventually showing highly overlapping and intersecting distributions. Thus, we conclude that within the investigated range of loading rates, the energetic coefficient of restitution can be assumed to be approximately constant. The anisotropic nature of granules makes the coefficient of restitution to be a parameter, only predictable with less precision. Numerous authors in the past have witnessed to this inability.[45–52] Thus, it is most appropriate to present the same using statistical distributions. In Figure 11, we summarize the energetic coefficient of restitution of all granules tested by compression tests, determined using both linear and non-linear approximations of the force-displacement behavior.

The values of the energetic coefficient of restitution determined by the non-linear approximation of the force-displacement behavior, is far more accurate than the one determined by the linear approximation, as it considers almost the exact trend. Recently Gilson et al.[53] reported that the Tomas model[42] predicts an overestimated value of the dissipated energy while modeling the cyclic contact behavior of inhomogeneous solids such as agglomerates. The authors

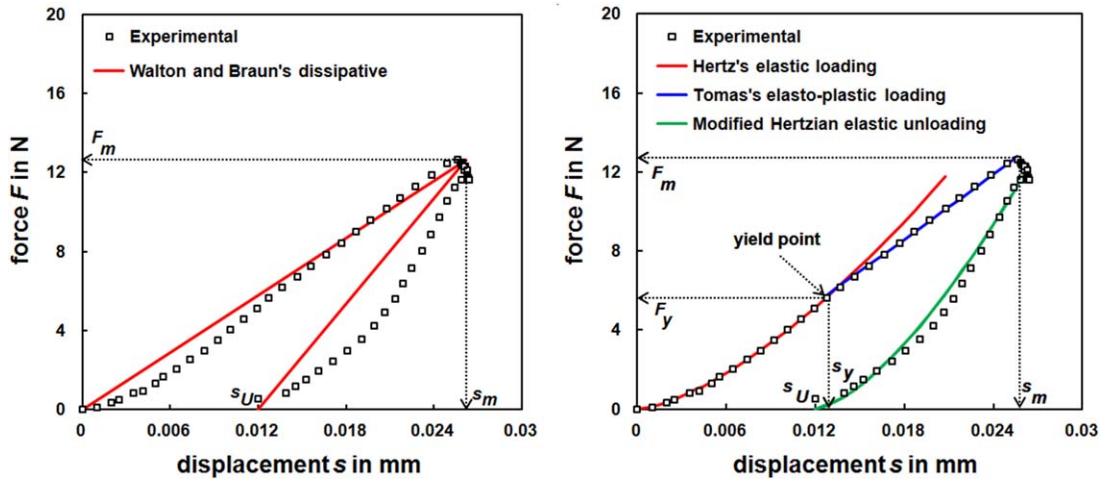

Figure 10. Experimental force-displacement curve approximated using (a) linear and (b) non-linear contact models.

[Color figure can be viewed in the online issue, which is available at wileyonlinelibrary.com.]

Table 3. Fitting Parameters used for Approximation of the Force-Displacement Curves

Granule Size (Mean Diameter) d_{50} in mm	Loading Rate v_L in mm/s	Maximum Force Level F_m in F_m/F_y	Fitting Parameter $\lambda_{el\text{-}pl}$ used for Tomas's Elasto-plastic Model[42]	Fitting Parameter $\vartheta_{el,U}$ used for Modified Hertzian Elastic Model[3]
1.75	0.01	0.5	–	5.6 ± 0.8
		1	0.93 ± 0.04	3.8 ± 0.5
		1.5	0.96 ± 0.04	3.1 ± 0.3
	0.02	0.5	–	5.3 ± 0.4
		1	0.97 ± 0.07	3.4 ± 0.6
		1.5	0.99 ± 0.07	3.4 ± 0.6
	0.08	0.5	–	3.8 ± 0.9
		1	0.97 ± 0.06	3.2 ± 0.7
		1.5	0.97 ± 0.07	2.7 ± 0.9
	0.15	0.5	–	2.4 ± 0.6
		1	1.03 ± 0.06	2.2 ± 0.5
		1.5	1.03 ± 0.05	2.3 ± 0.7
3.01	0.01	0.4	–	4.2 ± 0.8
		0.8	–	3.2 ± 0.4
		1.2	0.96 ± 0.05	2.9 ± 0.7
		1.6	0.95 ± 0.04	2.6 ± 0.7
	0.02	0.4	–	5.5 ± 1.4
		0.8	–	3.9 ± 2.2
		1.2	0.97 ± 0.05	2.8 ± 0.4
		1.6	0.98 ± 0.04	2.7 ± 0.8
	0.08	0.4	–	3.3 ± 1.1
		0.8	–	2.3 ± 0.8
		1.2	1.02 ± 0.07	2.3 ± 0.6
		1.6	1.01 ± 0.05	2.0 ± 0.3
	0.15	0.4	–	3.1 ± 1.0
		0.8	–	3.6 ± 1.8
		1.2	1.08 ± 0.11	2.5 ± 1.1
		1.6	1.04 ± 0.12	2.9 ± 1.0

presented the energetic coefficient of restitution as an exponential function considering the number of cycles. However, the model is based on the linear Walton–Braun[38] approach, assuming a constant contact stiffness during unloading and a residual displacement approached as a secant displacement. Although, the approach provides a basis to build further on to model the hardening behavior of granules during cyclic loading, the results presented in this article, clearly substantiate the validity of the non-linear Tomas model[42] for predicting the energetic characteristics of inhomogeneous anisotropic solids such as granules.

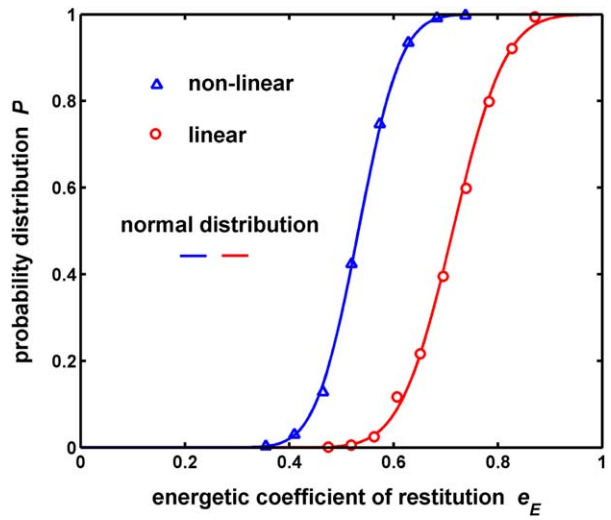

Figure 11. The energetic coefficient of restitution determined using linear and non-linear approximations of the force-displacement *F(s)* behavior.

[Color figure can be viewed in the online issue, which is available at wileyonlinelibrary.com.]

This interesting proposal probably arises from the much lower values of the energetic coefficient of restitution in comparison to the values of the kinematic coefficient of restitution reported by impact tests. The key reason for such a difference is the so-called strain rate, that is, rate of change of strain, which is significantly higher under dynamic impact loading (almost 10^5 or 10^6 orders of magnitude) than under quasi-static compressive loading. Furthermore, it is to be noted that impact loading is characterized by high dynamics, where there are significant energy losses which affect: kinetic energy absorption and recovery due to propagation of elastic stress waves at the instant of impact. Whereas, during compressive loading, the propagation of stress waves within the granule are slower, thereby causing a relatively more intense deformation (due to lesser stressing energy losses) than that realized by an energetically equivalent impact load.

Strain hardening besides contact zone

As each microscopic constituent uniquely defines a macrostate, the mechanical properties of the microscopic constituents are of significant importance to predict the macromechanical behavior. In general, during cyclic loading, significant mechanical interactions (which advance during plastic deformation) occur between structural inhomogeneities or so-called dislocations (pores, solid bridge bonds, microcracks, and defects) within the whole volume of the loaded granule.

In zeolite 4AK granules, localized granular hardening advances as a consequence of movement and subsequent accumulation of such dislocations (see Figure 12), during cyclic loading in an unmodified strain path. This mechanism advances by: an initial reorientation of dislocations into a

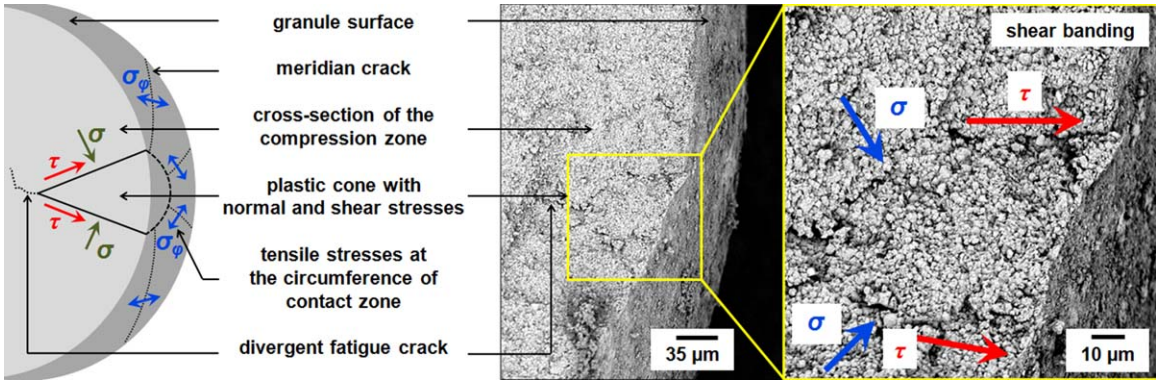

Figure 12. Schematic representation and SEM micrographs at 700 times and 2000 times enlargement of the cross-section of stressed contact zone showing strain hardening and cracking mechanism of zeolite 4AK granules during cyclic loading.

[Color figure can be viewed in the online issue, which is available at wileyonlinelibrary.com.]

preferred texture, with respect to the direction of the principal strain, expanding from the central plastic contact zone during the first two to three loads; followed by a sharply decreasing plastic strain due to interactions, interlocking, and interpenetration of the stress fields of dislocations, during the next 8–10 cycles; and ultimately resulting in the extinction

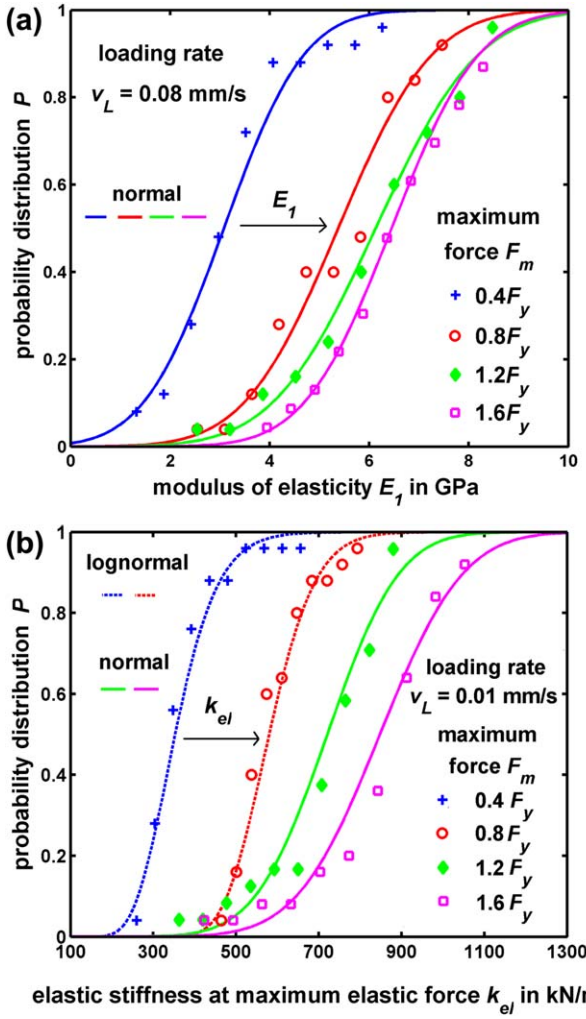

Figure 13. Changes in micromechanical properties during cyclic loading of a granule of size d_{50} = 3.01 mm (within the elastic range) in the (a) modulus of elasticity and the (b) elastic stiffness at maximum elastic force.

[Color figure can be viewed in the online issue, which is available at wileyonlinelibrary.com.]

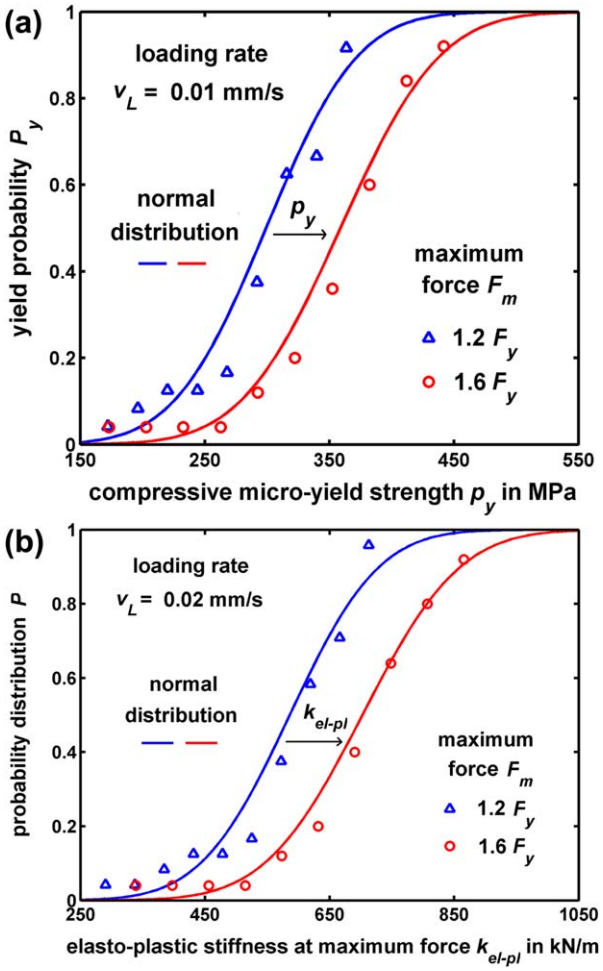

Figure 14. Changes in micromechanical properties during cyclic loading of a granule of size d_{50} = 3.01 mm (within the elasto-plastic range) in the (a) compressive micro-yield strength and the (b) elasto-plastic stiffness at maximum force.

[Color figure can be viewed in the online issue, which is available at wileyonlinelibrary.com.]

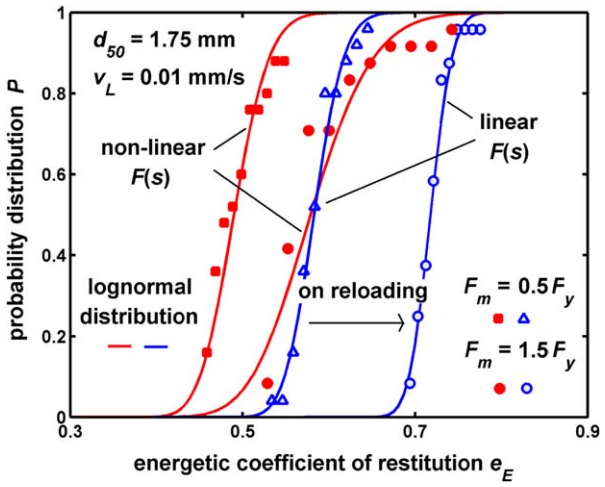

Figure 15. Energetic coefficient of restitution reflecting strain hardening during cyclic loading.

[Color figure can be viewed in the online issue, which is available at wileyonlinelibrary.com.]

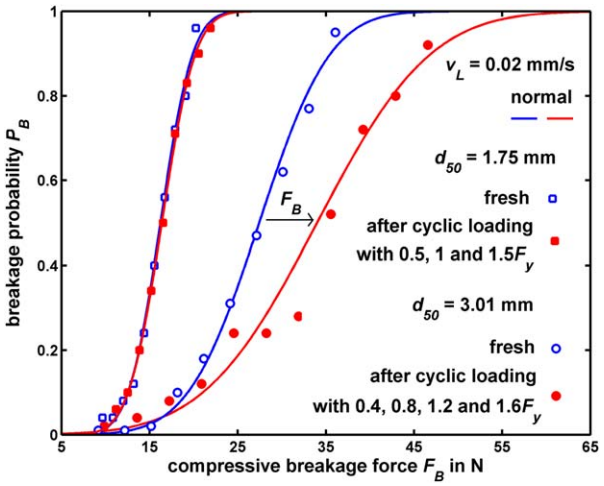

Figure 16. Comparison of the compressive breakage forces during monotonic loading until primary breakage of fresh and cyclically preloaded granules.

[Color figure can be viewed in the online issue, which is available at wileyonlinelibrary.com.]

of plastic strain in the overall contact zone due to achieving an accumulated critical amount of dislocations, where a completely stable plastically deformed plane (shear band) is formed in the direction of the strain path. Nevertheless, it is important to note that strain hardening occurs only in the direction of the principal strain forming a locally stable plastically deformed plane, in contrast to the general plastic yielding which progresses throughout the deforming contact zone.

In this study, we present localized granular hardening during cyclic loading with increasing compressive forces. Figures 13

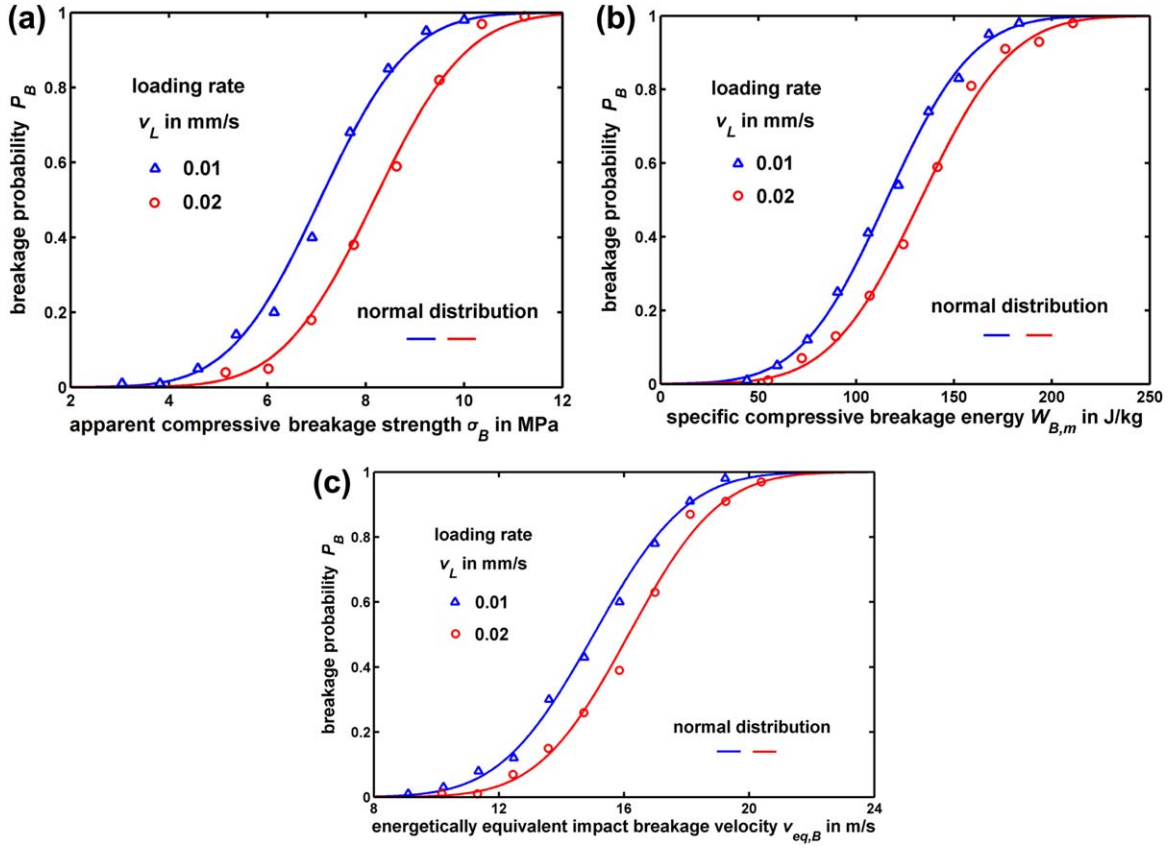

Figure 17. Breakage probability of a granule of size $d_{50} = 1.75$ mm expressed in terms of (a) apparent compressive breakage strength, (b) specific compressive breakage energy, and (c) its energetically equivalent impact breakage velocity.

[Color figure can be viewed in the online issue, which is available at wileyonlinelibrary.com.]

Table 4. Root-Mean-Square Error and Coefficient of Determination of Distributions Representing the Determined Micromechanical and Macromechanical Properties

Mechanical Property	Granule Size (Mean Diameter) d_{50} (mm)	Maximum Force Level F_m in F_m/F_y	Loading Rate v_L (mm/s)	Normal Distribution		Lognormal Distribution	
				RMS Error	R^2	RMS Error	R^2
Modulus of elasticity during loading E_1 in GPa	1.75	0.5	0.01	0.04	0.98	0.02	0.99
			0.02	0.03	0.98	0.02	0.99
			0.15	0.05	0.96	0.06	0.95
	3.01	0.8	0.01	0.06	0.94	0.05	0.96
		1.6		0.03	0.98	0.06	0.94
Elastic contact stiffness at maximum elastic force k_{el} in kN/m	1.75	1	0.02	0.04	0.98	0.05	0.96
			0.08	0.03	0.98	0.04	0.97
			0.15	0.05	0.96	0.06	0.95
	3.01	0.4	0.01	0.06	0.93	0.04	0.97
		0.8		0.06	0.95	0.05	0.97
		1.2		0.06	0.94	0.08	0.90
		1.6		0.05	0.96	0.07	0.92
Compressive micro-yield strength p_y in MPa	1.75	1	0.02	0.03	0.98	0.05	0.96
			0.08	0.03	0.98	0.03	0.98
			0.15	0.04	0.98	0.05	0.97
	3.01	1.2	0.01	0.06	0.95	0.08	0.91
		1.6		0.04	0.97	0.06	0.93
Elasto-plastic contact stiffness at maximum force $k_{el\text{-}pl}$ in kN/m	1.75	1	0.08	0.02	0.99	0.04	0.98
			0.15	0.05	0.95	0.07	0.92
	3.01	1.2	0.02	0.06	0.94	0.08	0.89
		1.6		0.04	0.97	0.06	0.94
Modulus of elasticity during unloading $E_{1,U}$ in GPa	1.75	1.5	0.01	0.05	0.97	0.05	0.96
			0.08	0.02	0.99	0.05	0.95
			0.15	0.05	0.96	0.07	0.92
	3.01	0.8	0.01	0.04	0.97	0.03	0.98
		1.6		0.02	0.99	0.05	0.95
Energetic coefficient of restitution e_E determined by linear approximation of the $F(s)$ function	1.75	0.5	0.01	0.05	0.95	0.05	0.96
		1.5		0.03	0.98	0.03	0.98
	Of all sizes	For all force levels	At all loading rates	0.01	0.99	0.02	0.99
Energetic coefficient of restitution e_E determined by nonlinear approximation of the $F(s)$ function	1.75	0.5	0.01	0.08	0.93	0.07	0.94
		1.5		0.09	0.87	0.08	0.89
	Of all sizes	For all force levels	At all loading rates	0.00	0.99	0.01	0.99
Compressive breakage force F_B in N	1.75	Until primary breakage of fresh granules	0.02	0.01	0.99	0.02	0.99
		Until primary breakage of pre-loaded granules		0.02	0.99	0.03	0.98
	3.01	Until primary breakage of fresh granules		0.02	0.99	0.04	0.97
		Until primary breakage of pre-loaded granules		0.05	0.96	0.08	0.91
Apparent compressive breakage strength σ_B in MPa	1.75	Until primary breakage	0.01	0.02	0.98	0.04	0.97
			0.02	0.02	0.99	0.03	0.98
Specific compressive breakage energy $W_{B,m}$ in J/kg	1.75	Until primary breakage	0.01	0.02	0.99	0.03	0.98
			0.02	0.03	0.98	0.04	0.97
Energetically equivalent impact breakage velocity $v_{eq,B}$ in m/s	1.75	Until primary breakage	0.01	0.01	0.99	0.03	0.98
			0.02	0.02	0.99	0.04	0.97

and 14 show the changes in micromechanical properties within the elastic and the elasto-plastic ranges, respectively.

A clearer picture of strain hardening can be understood from the evaluated energetic coefficient of restitution which clearly progresses (see Figure 15) due to a decreasing contribution of the plastic strain to the total observed deformation, even with an increasing compressive force with every cycle.

Concurrently, during movement and accumulation of dislocations, fatigue cracks (see Figure 12) nucleate, propagate, and grow perpendicularly (in a divergent fashion) to the direction of the maximum principal strain, from the stabilizing localized plastically deformed contact planes, as a result of residual stresses, eventually resulting in primary breakage by fatigue. Nevertheless, granules are locally hardened during cyclic loading, and thereby break at compressive force levels higher than the mean breakage force of fresh granules, especially during compression in the unmodified strain path (see Figure 16).

However, on modifying the strain path, that is, by stressing at a new contact different from the cyclically loaded

one, granules break at lower forces. This establishes the fact that loading a granule increases its strength in the direction of the principal strain, however, practically advancing its breakage probability as granules are stressed at random contacts during industrial operations.

Breakage probability

All granules exhibit a dominantly brittle breakage behavior evidently noticeable from the steeply decreasing compressive force instantaneously following primary breakage, as elaborately discussed in previous communications.[6,8,9] Adding on, we present the breakage probability (Figure 17) at different loading rates using distribution functions of the apparent compressive breakage strength, the specific compressive breakage energy and its energetically equivalent impact breakage velocity.

The apparent compressive breakage strength σ_B is approximated by

$$\sigma_B = \frac{F_B}{A_1} \approx \frac{4}{\pi}\frac{F_B}{d_1^2} \tag{13}$$

with F_B the force at primary breakage and A_1 the cross-sectional area of the granule.

The specific compressive breakage energy $W_{B,m}$ (related to the granule mass m_1) is given by

$$W_{B,m} = \frac{W_B}{m_1} = \frac{1}{m_1}\int_{s_0}^{s_B} F(s)ds \tag{14}$$

with W_B the total compressive energy absorption until primary breakage and s_B the displacement at primary breakage. An energetically equivalent impact breakage velocity $v_{eq,B}$, that is, an impact load of equivalent kinetic energy is given by

$$v_{eq,B} = \sqrt{2\frac{W_B}{m_1}} = \sqrt{2W_{B,m}} \tag{15}$$

The results clearly imply that at higher displacement-controlled loading rates, higher loads are required to realize equivalent breakage probability as achieved at lower displacement-controlled loading rates.

The root-mean-square error and the coefficient of determination values for every distribution described in this article are presented in Table 4.

Conclusions

The presented results in the form of statistical distributions, present a highly precise representation of the distributed granular micromechanical, energetic and breakage characteristics, which may be used to optimize granulation techniques for future production, and industrial handling operations (particularly with respect to transportation and storage) of granules, to avoid undesired deformation and breakage. In the present state of the art, predicting the mechanical behavior of bulk assemblies based on the mechanical behavior of single (constituent) granules is highly complex, due to the presently indeterminable realistic packing state of almost always polydisperse granules. Nevertheless, an empirical scale-up criteria may be approached by comparing the mechanical behavior of individual granules with that of a granule bed under isentropic compression.

The results described in this article, clearly show that the loading rate is a parameter that influences the compression behavior of zeolite 4AK granules. At higher displacement-controlled loading rates, higher compressive loads are required to realize equivalent deformation and breakage probability in comparison to those achieved by loads at lower displacement-controlled loading rates. The observed effects are expected to intensify during compression of zeolite 4AK granules in the moist and wet states.

The presented evaluations provide a yardstick to understand and also serve as a foundation to comprehensively investigate the rate-dependent viscous deformation of zeolite 4AK granules by evaluating a model-based damping coefficient which describes the viscous damping behavior. Furthermore, the results may be used to calibrate representative granules using the discrete element method, and numerically simulate the compression behavior under different displacement-controlled loading rates.

Acknowledgments

This work was supported by the K 32-2 Graduate Funding of the State (GVBI. LSA No. 35/2001) from the Ministry of Science and Economy in Saxony-Anhalt, Federal Republic of Germany. We thank the Chemiewerk Bad Köstritz GmbH, and in particular Dr. K. Schumann for the valuable discussions and provision of the tested granules.

Notation

Roman symbols

A_1 = cross-sectional area of the granule, mm^2
A_{pl} = circular inner plastic contact area, mm^2
A_{tot} = total contact area, mm^2
d_1 = diameter of the granule, mm
d_{50} = mean diameter of granules which form 50% of the total sample mass, mm
E^* = effective modulus of elasticity of the granule and the flat stiff contact, GPa
E_1 = modulus of elasticity of the granule during loading, GPa
$E_{1,U}$ = modulus of elasticity of the granule during unloading, GPa
E_2 = modulus of elasticity of the flat stiff wall, GPa
e = coefficient of restitution, dimensionless
e_E = energetic coefficient of restitution, dimensionless
F_B = force at primary breakage, N
F_{el} = elastic contact force during loading, N
$F_{el\text{-}pl}$ = elasto-plastic contact force during loading, N
$F_{el,U}$ = elastic contact force during unloading, N
F_L = loading force, N
F_m = maximum defined force level, N
F_U = unloading force, N
F_y = force at yield point, N
k_{el} = elastic contact stiffness, kN/m
$k_{el\text{-}pl}$ = elasto-plastic contact stiffness, kN/m
k_L = loading stiffness, kN/m
k_U = unloading stiffness, kN/m
m_1 = mass of the granule, g
p_y = compressive micro-yield strength, MPa
P = probability distribution function, dimensionless
P_B = breakage probability distribution function, dimensionless
P_y = yield probability distribution function, dimensionless
Q_3 = mass-related granule size distribution function, dimensionless
R^* = effective radius of curvature of the granule and of the flat stiff contact, mm
R_1 = radius of curvature of the granule, mm
R_2 = radius of curvature of the flat stiff contact, indeterminable
S_m = specific surface area of the granule, m^2/kg
s = displacement, mm
s_B = displacement at primary breakage, mm
s_m = displacement corresponding to maximum normal force, mm

s_U = residual displacement at unloading corresponding to zero loading force, mm
s_y = displacement at yield point, mm
$v_{eq,B}$ = energetically equivalent impact velocity initiating primary breakage, m/s
v_i = impact velocity, m/s
v_L = displacement-controlled constant loading rate, mm/s
v_r = rebound velocity, m/s
W_B = compressive energy required to initiate primary breakage, J
$W_{B,m}$ = specific compressive breakage energy, J/kg
$W_{el,U}$ = elastic strain energy recovery during unloading, J
$W_{kin,i}$ = kinetic impact energy, J
$W_{kin,r}$ = kinetic rebound energy recovery, J
W_{tot} = total compressive energy absorption during loading, J

Greek letters

δ = displacement of the granule at a single contact, mm
ε = porosity, %
κ_A = elasto-plastic contact area coefficient, dimensionless
$\lambda_{el\text{-}pl}$ = fitting parameter of Tomas's elasto-plastic model,[42] dimensionless
ν_1 = Poisson's ratio of the granule, dimensionless
ν_2 = Poisson's ratio of the flat stiff wall, dimensionless
π = mathematical constant, dimensionless
ρ_g = granule density, kg/m^3
ρ_s = solid (true) density, kg/m^3
σ_B = apparent compressive breakage strength, MPa
σ_c = compressive stress, MPa
σ_φ = tensile stress, MPa
τ = shear stress, MPa
ψ = sphericity, dimensionless
$\vartheta_{el,U}$ = fitting parameter of the proposed modified Hertzian elastic model, dimensionless

Literature Cited

1. Ennis BJ. Unto dust shalt thou return. In: Proceedings of Powders and Grains, AA Balkema Publishers, North Carolina, 1997:13–24.
2. Rumpf H. Grundlagen und Methoden des Granulierens (Fundamentals and methods of granulation). *Chem Ing Tech*. 1958;30:144–158.
3. Litster JD, Ennis BJ. *The Science and Engineering of Granulation Processes*. Dordrecht: Kluwer Academic Publishers, 2004.
4. Tomas J. Mechanical Process Engineering. Lecture manuscript, Otto von Guericke University of Magdeburg. Available at: www.mvt.ovgu.de, accessed on July 7, 2014.
5. Antonyuk S. Deformations- und Bruchverhalten von kugelförmigen Granulaten bei Druck- und Stoßbeanspruchung (Deformation and breakage behavior of spherical granules by compression and impact stressing). Dissertation (PhD Thesis), Germany: Otto von Guericke University of Magdeburg, Docupoint Verlag, Barleben, 2006.
6. Antonyuk S, Tomas J, Heinrich S, Mörl L. Breakage behaviour of spherical granulates by compression. *Chem Eng Sci*. 2005;60:4031–4044.
7. Antonyuk S, Heinrich S, Tomas J, Deen NG, van Buijtenen MS, Kuipers JAM. Energy absorption during compression and impact of dry elastic-plastic spherical granules. *Granul Matter*. 2010;12:15–47.
8. Müller P, Antonyuk S, Tomas J. Influence of moisture content on the compression behavior of granules. *Chem Eng Technol*. 2011;34:1543–1550.
9. Müller P, Tomas J. Compression behavior of moist spherical zeolite 4A granules. *Chem Eng Technol*. 2012;35:1677–1684.
10. Russell A, Müller P, Tomas J. Quasi-static diametrical compression of characteristic elastic-plastic granules: Energetic aspects at contact. *Chem Eng Sci*. 2014;114:70–84.
11. Gorham DA. The effect of specimen dimensions on high strain rate compression measurements of copper. *J Phys D: Appl Phys*. 1991;24:1489–1492.
12. Vogel L, Peukert W. Breakage behaviour of different materials—construction of a mastercurve for the breakage probability. *Powder Technol*. 2003;129:101–110.
13. Zhang X-P, Wong LNY. Loading rate effects on cracking behavior of flaw-contained specimens under uniaxial compression. *Int J Fracture*. 2013;180:93–110.
14. Schönert K. Breakage of spheres and circular discs. *Powder Technol*. 2004;143–144:2–18.
15. Tomas J, Schreier M, Gröger T, Ehlers S. Impact crushing of concrete for liberation and recycling. *Powder Technol*. 1999;105:39–51.
16. Rumpf H. Physical aspects of comminution and a new formulation of a law of comminution. *Powder Technol*. 1973;7:145–159.
17. Tavares LM, King RP. Single-particle fracture under impact loading. *Int J Miner Process*. 1998;54:1–28.
18. Tavares LM. Breakage of single particles: quasi-static. In: Salman AD, Ghadiri M, Hounslow M, editors. *Handbook of Powder Technology, Particle breakage*, Vol. 12. The Netherlands: Elsevier BV, 2007:1–68.
19. Qi C, Wang M, Qian Q. Strain-rate effects on the strength and fragmentation size of rocks. *Int J Impact Eng*. 2009;36:1355–1364.
20. Salman AD, Gorham DA. The fracture of glass spheres. *Powder Technol*. 2000;107:179–185.
21. Tang CA, Liu HY, Zhu WC, Yang TH, Li WH, Song L, Lin P. Numerical approach to particle breakage under different loading conditions. *Powder Technol*. 2004;143–144:130–143.
22. Khandelwal M, Ranjith PG. Behaviour of brittle material in multiple loading rates under uniaxial compression. *Geotech Geol Eng*. 2013;31:1305–1315.
23. Iveson SM. Fundamentals of granule consolidation and deformation. PhD Thesis, Australia: University of Queensland, 1997.
24. Couroyer C, Ning Z, Ghadiri M. Distinct element analysis of bulk crushing: effect of particle properties and loading rate. *Powder Technol*. 2000;109:241–254.
25. Franks GV, Lange, FF. Plastic flow of saturated alumina powder compacts: Pair potential and strain rate. *AIChE J*. 1999;45:1830–1835.
26. Khanal M. Simulation of crushing dynamic of an aggregate-matrix composite by compression and impact stressings. Dissertation (PhD Thesis), Germany: Otto von Guericke University of Magdeburg, Docupoint Verlag, Barleben, 2005.
27. Cheong YS, Adams MJ, Routh AF, Hounslow MJ, Salman AD. The production of binderless granules and their mechanical characteristics. *Chem Eng Sci*. 2005;60:4045–4053.
28. Samimi A, Hassanpour A, Ghadiri M. Single and bulk compressions of soft granules: experimental study and DEM evaluation. *Chem Eng Sci*. 2005;60:3993–4004.
29. Al Mahdi R, Nasirpour A, Banon S, Scher J, Desobry S. Morphological and mechanical properties of dried skimmed milk and wheat flour mixtures during storage, *Powder Technol*. 2006;163:145–151.
30. Smith RM. Wet granule breakage in high shear mixer granulators. PhD Thesis, Australia: The University of Queensland, 2008.
31. Nguyen, VB, Wang CX, Thomas CR, Zhang Z. Mechanical properties of alginate microspheres determined by microcompression and finite element modelling. *Chem Eng Sci*. 2009;64:821–829.
32. Aman S, Tomas J, Kalman H. Breakage probability of irregularly shaped particles. *Chem Eng Sci*. 2010;65:1503–1512.
33. Müller P. Druck-, Stoß- und Bruchverhalten feuchter kugelförmiger Granulate (Compression, impact and breakage behavior of moist spherical granules). Dissertation (PhD Thesis), Germany: Otto von Guericke University of Magdeburg, Docupoint Verlag, Barleben, 2011.
34. Wiącek J, Molenda M, Horabik J, Ooi JY. Influence of grain shape and interangular friction on material behavior in uniaxial compression: experimental and DEM modeling. *Powder Technol*. 2012;217:435–442.
35. Hanley KJ, O'Sullivan C, Byrne EP, Cronin K. Discrete element modelling of quasi-static uniaxial compression of individual infant formula agglomerates. *Particuology*. 2012;10:523–531.
36. Portnikov D, Kalman H, Aman S, Tomas J. Investigating the testing procedure limits for measuring particle strength distribution. *Powder Technol*. 2013;237:489–496.
37. Schumann K, Brandt A, Unger B, Scheffler F. Bindemittelfreie zeolithische Molekularsiebe der Typen LTA und FAU (Binderless zeolite molecular sieves of the types LTA and FAU). *Chem Ing Tech*. 2011;83:2237–2243.
38. Walton OR, Braun RL. Viscosity, granular-temperature, and stress calculations for shearing assemblies of inelastic, frictional disks. *J Rheol*. 1986;30:949–980.
39. Hertz H. Über die Berührung fester elastischer Körper (About the contact of firm elastic solids). *J Reine Angew Math*. 1882;92:156–171.
40. Johnson KL. *Contact Mechanics*. Cambridge: Cambridge University Press, 1985.
41. Tomas J. Produkteigenschaften ultrafeiner Partikel - Mikromechanik, Fließ- und Kompressionsverhalten kohäsiver Pulver (Product properties of ultrafine particles - Micromechanical, flow and compression behavior of cohesive powders). Germany: Sächsischen Akademie der Wissenschaften zu Leipzig, 2009.
42. Tomas J. Adhesion of ultrafine particles—a micromechanical approach. *Chem Eng Sci*. 2007;62:1997–2010.

43. Tomas J. Assessment of mechanical properties of cohesive particular solids–Part 1: particle contact constitutive model. *Part Sci Technol*. 2001;19:95–110.
44. Mader-Arndt K, Kutelova Z, Fuchs R, Meyer J, Staedler T, Hintz W, Tomas J. Single particle contact versus particle packing behavior: model based analysis of chemically modified glass particles. *Granul Matter*. 2014;16:359–375.
45. Müller P, Antonyuk S, Stasiak M, Tomas J, Heinrich S. The normal and oblique impact of three types of wet granules. *Granul Matter*. 2011;13:455–463.
46. Thornton C. Coefficient of restitution for collinear collisions of elastic-perfectly plastic spheres. *J Appl Mech*. 1997;64:383–386.
47. Fu J, Adams MJ, Reynolds GK, Salman AD, Hounslow MJ. Impact deformation and rebound of wet granules. *Powder Technol*. 2004; 140:248–257.
48. Wong CK, Rao SM, Wang C-H. Pneumatic conveying of granular solids in horizontal and inclined pipes. *AIChE J*. 2004;50:1729–1745.
49. Liu LX, Litster JD, Iveson SM, Ennis BJ. Coalescence of deformable granules in wet granulation processes. *AIChE J*. 2004;46: 529–539.
50. Sudah OS, Arratia PE, Alexander A, Muzzio FJ. Simulation and experiments of mixing and segregation in a tote blender. *AIChE J*. 2005;51:836–844.
51. Iddir H, Arastoopour H. Modeling of multitype particle flow using the kinetic theory approach. *AIChE J*. 2005;51:1620–1632.
52. Mangwandi C, Cheong YS, Adams MJ, Hounslow MJ, Salman AD. The coefficient of restitution of different representative types of granules. *Chem Eng Sci*. 2007;62:437–450.
53. Gilson L, Kozhar S, Antonyuk S, Bröckel U, Heinrich S. Contact models based on experimental characterization of irregular shaped, micrometer-sized particles. *Granul Matter*. 2014;16:313–326.

Manuscript received Mar. 27, 2014, and revision received July 8, 2014.